Global retrieval of columnar aerosol single scattering albedo from space-based observations

R.-M. Hu,[1] R. V. Martin,[1,2] and T. D. Fairlie[3,4]

Received 28 October 2005; revised 12 July 2006; accepted 12 September 2006; published 20 January 2007.

[1] We retrieve the global distribution of columnar single scattering albedo (ω_0) by taking advantage of the high sensitivity of satellite measurements at ultraviolet channels by the Total Ozone Mapping Spectrometer (TOMS) to both aerosol optical depth and ω_0 and the high sensitivity of satellite measurements at visible channels by the Moderate Resolution Imaging Spectroradiometer (MODIS) to aerosol optical depth. A radiative transfer model (LIDORT) is used to calculate the local ω_0 that reproduces the TOMS aerosol index, when constrained by MODIS aerosol optical depth and by relative vertical profiles from a global chemical transport model (GEOS-CHEM). The simulated aerosol profiles are evaluated with lidar measurements of aerosol extinction. The retrieved ω_0 at 360 nm is near 1 over the remote ocean, in contrast with values of 0.75 to 0.9 over regions dominated by biomass burning and mineral dust aerosol. The retrieval uncertainty is 15%. We validate our retrieval with measurements from the Aerosol Robotic Network (AERONET); the correlation coefficient, slope, and intercept are 0.75, 0.99, and 0.02 respectively.

Citation: Hu, R.-M., R. V. Martin, and T. D. Fairlie (2007), Global retrieval of columnar aerosol single scattering albedo from space-based observations, *J. Geophys. Res.*, *112*, D02204, doi:10.1029/2005JD006832.

1. Introduction

[2] The lack of detailed knowledge of aerosol single scattering albedo (ω_0), the fraction of intercepted radiation that is scattered, is one of the largest uncertainties in climate forcing assessments [*Intergovernmental Panel on Climate Change*, 2001]. A decrease in ω_0 from 0.9 to 0.8 can often change the sign of radiative forcing from negative to positive, depending on the albedo of the underlying surface and the altitude of the aerosols [*Hansen et al.*, 1997]. Modeling of aerosol absorption is complicated by chemical composition, size distribution and aerosol morphology. Emissions of carbonaceous compounds (soot) from biomass burning and industrial pollution remain a major source of uncertainty affecting the aerosol absorption [*Chylek et al.*, 1995; *Haywood and Shine*, 1995; *Penner et al.*, 1998; *Li and Kou*, 1998; *Ackerman et al.*, 2000; *Ramanathan et al.*, 2001; *Kaufman et al.*, 2002b]. A global continuous measurement of ω_0 could reduce significantly this uncertainty.

[3] Spaceborne measurements provide an opportunity to capture the large spatial and temporal variation of ω_0 [*King et al.*, 1999]. Satellite instruments such as MODIS that observe backscattered visible and infrared radiances reveal a wealth of information about aerosol optical depth [*Kaufman et al.*, 2002b]; however, they are insensitive to ω_0 over dark surfaces [*Kaufman et al.*, 1997]. Over the oceans, Sun glint can be used as a bright background against which aerosol absorption can be measured from space [*Kaufman et al.*, 2002a]. Similarly, Rayleigh scattering acts as a bright background in the ultraviolet so that the Total Ozone Mapping Spectrometer (TOMS) aerosol index is sensitive to the combination of aerosol optical depth and ω_0 [*Herman et al.*, 1997; *Torres et al.*, 1998].

[4] *Torres et al.* [1998, 2005] pioneered the concept of retrieving ω_0 from satellite measurements at ultraviolet wavelengths. Their retrieval of ω_0 employs the magnitude of the backscattered radiance in the ultraviolet, the ratio of the two TOMS aerosol channels, and assumptions about the aerosol vertical profile. The magnitude of backscattered radiance is sensitive to subpixel cloud contamination over the TOMS field of view. The effect of clouds will be reduced in a forthcoming retrieval of ω_0 from the Ozone Monitoring Instrument which offers five times better spatial resolution than Earth Probe (EP) TOMS [*Torres et al.*, 2002]. *Ginoux and Torres* [2003] established an empirical expression for the aerosol index as a function of surface pressure, ω_0, aerosol optical depth, and the altitude of the aerosol layer. *Colarco et al.* [2002] developed a retrieval of aerosol single scattering albedo that is independent of absolute backscattered radiance, by combining the TOMS aerosol index with constraints on aerosol optical depth from a chemical transport model.

[5] We extend these approaches here using cloud-filtered observations of aerosol optical depth from the MODIS satellite instrument and aerosol vertical profiles from a

[1]Department of Physics and Atmospheric Science, Dalhousie University, Halifax, Nova Scotia, Canada.
[2]Also at Harvard-Smithsonian Center for Astrophysics, Cambridge, Massachusetts, USA.
[3]NASA Langley Research Center, Hampton, Virginia, USA.
[4]Also at Department of Earth and Planetary Sciences and Division of Engineering, Harvard University, Cambridge, Massachusetts, USA.

0148-0227/07/2005JD006832

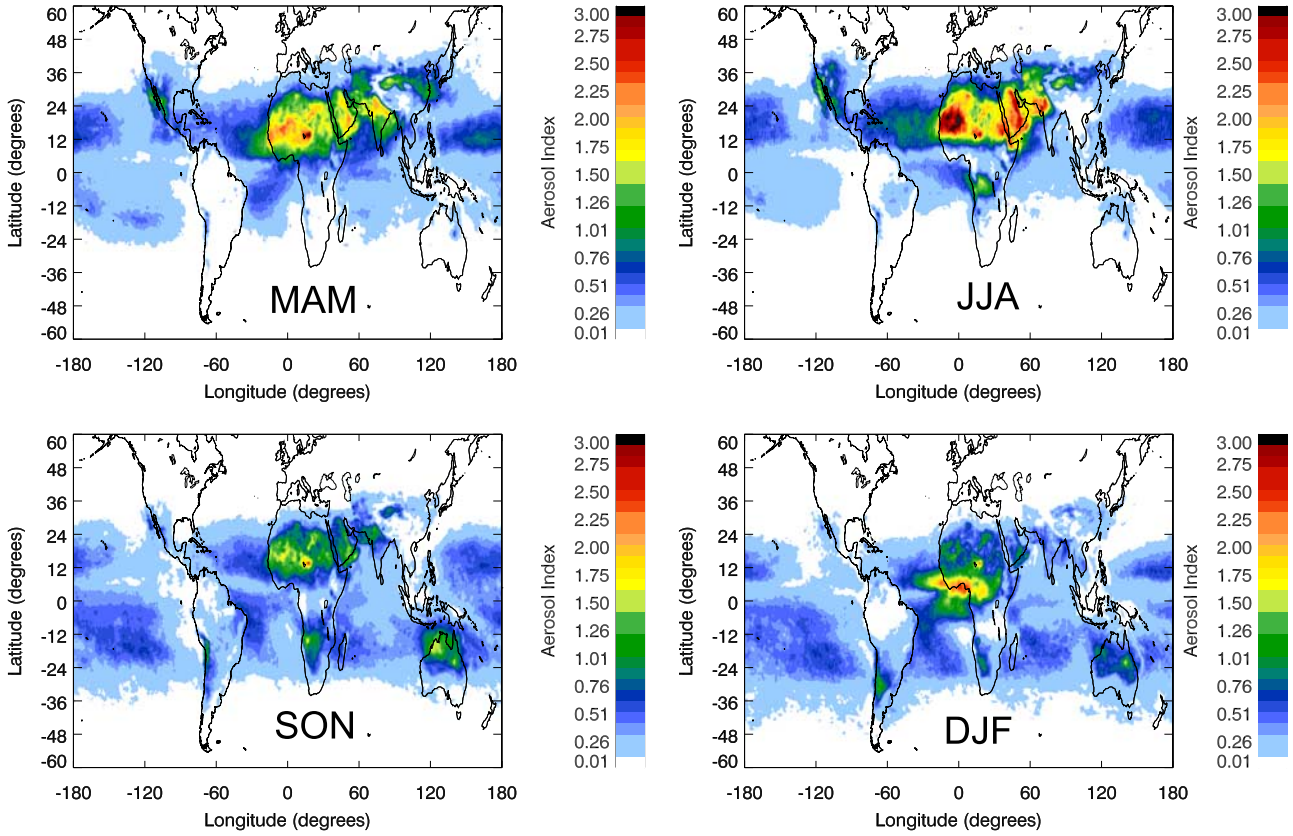

Figure 1. Seasonally averaged aerosol index from the TOMS satellite instrument for March–May 2000 (MAM), June–August 2000 (JJA), September–November 2000 (SON), and December 2000 to February 2001 (DJF). Scenes where the reflectivity at 331 nm exceeds 0.2 have been excluded from the average to reduce the effects of clouds and snow.

global chemical transport model (GEOS-CHEM). We use the vector discrete ordinate radiative transfer model VLIDORT (with polarization) [*Natraj et al.*, 2007; R. J. D. Spurr, VLIDORT: A linearized pseudo-spherical vector discrete ordinate radiative transfer model for forward model and retrieval studies in multilayer, multiple scattering media, submitted to *Journal of Quantitative Spectroscopy and Radiative Transfer*, 2006, hereinafter referred to as Spurr, submitted manuscript, 2006] for the calculation of the total backscatter radiance. The retrieval of the global distribution of ω_0 is done using spectral matching based on look-up tables of simulated earthshine spectra for a range of the ultraviolet, viewing geometries, atmospheric and surface conditions. The retrieved ω_0 values are then validated with ground-based retrievals from AERONET [*Dubovik et al.*, 2002] and in situ measurements.

2. Methodology

[6] The backscattered radiance measured by satellite sensors is composed of contributions from the atmosphere and surface. Scattering and absorption by aerosols produces a signal in the backscattered radiance that can be used to retrieve the aerosol properties. Our retrieval of ω_0 requires prior information described below. The TOMS aerosol index is the ω_0 sensitive measurement. Independent information on aerosol optical depth and on the relative aerosol vertical profile are used to constrain other parameters to which the TOMS aerosol index is sensitive.

2.1. TOMS Aerosol Index

[7] The EP TOMS satellite instrument was launched in July 1996 into a Sun-synchronous orbit with an equator crossing time of 1115 LT. The field of view is 40 km by 40 km in the nadir and increases with scan angle. The TOMS aerosol index (AI) measures the spectral contrast at two different ultraviolet wavelengths [*Herman et al.*, 1997; *Torres et al.*, 1998]:

$$AI = 100\left[\log_{10}\left[\frac{I_{360}}{I_{331}}\right]_{\text{meas}} - \log_{10}\left[\frac{I_{360}\left(R_{331}^{\text{meas}}\right)}{I_{331}\left(R_{331}^{\text{meas}}\right)}\right]_{\text{calc}}\right] \quad (1)$$

where I_{331}^{meas} and I_{360}^{meas} are the backscattered radiances measured at 331 nm and 360 nm. $I_{331}(R_{331}^{\text{meas}})_{\text{calc}}$ and $I_{360}(R_{331}^{\text{meas}})_{\text{calc}}$ are the backscattered radiances calculated with reflectance R_{331} at reference wavelength 331nm. We use here the EP TOMS version 8 level 2 data.

[8] Figure 1 shows the cloud-filtered aerosol index for different seasons. The aerosol index increases with aerosol absorption, aerosol abundance, and aerosol altitude [*Herman et al.*, 1997; *Torres et al.*, 1998; *Ginoux and Torres*, 2003; *de Graaf et al.*, 2005]. The largest values are found over regions with an abundance of mineral dust or

soot which absorbs in the ultraviolet. The aerosol index reaches a seasonal maximum over the Sahara during summer, associated with surface cyclones that erode particles from topographic depressions in desert regions and with intense solar heating that transports particles into the free troposphere through dry convection [*Herman et al.*, 1997; *Ginoux et al.*, 2001; *Ginoux and Torres*, 2003]. The seasonal variation in the aerosol index over biomass burning regions is most apparent over South America [*Hsu et al.*, 1996] and central Africa [*Herman et al.*, 1997]. The aerosol index is also sensitive to clear water absorption [*Litjens et al.*, 1999; *Torres et al.*, 2005] which contributes to enhancements over the Pacific Ocean near 15°N during MAM and JJA, and near 15°S during SON and DJF. Ocean color retrievals [i.e., *O'Reilly et al.*, 1998] reveal low chlorophyll abundance in these regions. Small nonabsorbing aerosols yield a negative aerosol index and large nonabsorbing aerosols produce null values of the aerosol index. Low values of the aerosol index are found over regions with a high sulfate burden [*Chin et al.*, 2000a, 2000b] such as the northern midlatitudes and regions with enhanced sea salt such as the high latitude oceans [*Gong et al.*, 1997]. Similarly, the aerosol index is insensitive to clouds since they produce little spectral contrast in the ultraviolet. Absorbing aerosols can be detected over snow, ice and clouds [*Hsu et al.*, 1999].

2.2. Aerosol Optical Depth From MODIS

[9] The MODIS instrument was launched on board the Terra satellite in December 1999 into a Sun-synchronous orbit with an equator crossing time of 1030 LT. Aerosol optical depth is determined from MODIS measurements over ocean [*Tanré et al.*, 1997] and dark land surfaces [*Kaufman et al.*, 1997] through observations at visible and infrared wavelengths. Cloud screening [*Martins et al.*, 2002] occurs over both surface types. The 500 m spatial resolution of MODIS greatly reduces subpixel cloud contamination. Observations over bright land surfaces are rejected. The optical depth determined by matching with the values computed with precalculated look-up tables is accurate to 20% ± 0.05 over land [*Chu et al.*, 2002] and to 5% ± 0.03 over ocean [*Remer et al.*, 2002].

[10] Relating the MODIS observations of aerosol optical depth to the TOMS aerosol index involves accounting for their different wavelengths of observation. The shortest wavelength at which aerosol optical depth is available from MODIS is 470 nm. AERONET collects extensive optical and microphysical information about aerosols through worldwide ground-based Sun and sky scanning radiometers [*Holben et al.*, 1998]. A filter wheel allows measurements in up to 8 spectral bands centered at 0.34, 0.38, 0.44, 0.56, 0.67, 0.87, 0.94, and 1.02 μm. Typically, the Ångström exponent α is defined by

$$\alpha = -\ln(\tau_{\lambda_1}/\tau_{\lambda_2})/\ln(\lambda_1/\lambda_2) \quad (2)$$

where τ_{λ_1} and τ_{λ_2} are the optical depths measured at two wavelengths. We spatially interpolate the Ångström exponents determined from AERONET measurements at 380 nm and 440 nm to produce a global field. This approach would be improved with additional information on the spatial variation in the Ångström exponent. Errors associated with this approach are discussed in section 4.

[11] Figure 2 presents the aerosol optical depth at 360 nm that we have determined from MODIS aerosol optical depth at 470 nm and Ångström exponents from AERONET. Values greater than one are found over regions with a high abundance of submicron aerosols. High SO_2 oxidation rates during summer contribute to seasonal enhancements in aerosol optical depth over the eastern United States, Europe, and east Asia [*Chin et al.*, 2000a, 2000b]. The seasonal variation in aerosol optical depth over Africa is driven by biomass burning [*Chu et al.*, 2003]. Mineral dust contributes to enhancements over the northern tropical Atlantic downwind of the Sahara, especially during JJA [*Kaufman et al.*, 2005]. High values of aerosol optical depth are seen over East Asia and the western Pacific Ocean during spring and summer, associated with dust storms and industrial pollution [*Chu et al.*, 2005]. Most deserts or snow/ice regions are excluded due to high surface reflectivity [*Chu et al.*, 2002]. Comparison with Figure 1 shows that the TOMS aerosol index is sensitive to absorbing aerosols (i.e., over regions of biomass burning and mineral dust), but insensitive to scattering aerosols (i.e., over industrial regions).

2.3. Aerosol Profiles From the GEOS-CHEM Model

[12] Our retrieval of ω_0 requires independent information on the aerosol profile to account for the altitude dependence of ultraviolet measurements. Given the lack of observational data at the global scale, we use aerosol profiles calculated with the GEOS-CHEM chemical transport model [*Bey et al.*, 2001; *Park et al.*, 2004, 2005; *Alexander et al.*, 2005]. The model is driven by assimilated meteorological data from the Goddard Earth Observing System (GEOS-3) at the NASA Global Modeling and Assimilation Office (GMAO). Meteorological data for 2000 are available with 6-hour temporal resolution (3-hour resolution for surface variables and mixing depths), $1^\circ \times 1^\circ$ horizontal resolution, and 48 sigma vertical layers. We use version 7-01-02, http://www-as.harvard.edu/chemistry/trop/geos/index.html) at $2^\circ \times 2.5^\circ$ horizontal resolution. The lowest five model layers are centered at 10, 50, 100, 200, and 400 m above the local surface.

[13] The GEOS-CHEM aerosol simulation includes the sulfate-nitrate-ammonium system, black carbon, primary organics, mineral dust, and sea salt. The mineral dust simulation is based on the Dust Entrainment and Deposition (DEAD) scheme of *Zender et al.* [2003a, 2003b] as implemented by *Fairlie et al.* [2006]. The simulation of carbonaceous aerosols treats hydrophobic and hydrophilic aerosols as separate transported species [*Park et al.*, 2005]. The aerosol and oxidant simulations are coupled through formation of sulfate and nitrate heterogeneous chemistry [*Jacob*, 2000] and aerosol effects on photolysis rates [*Martin et al.*, 2003]. Wet deposition includes contributions from scavenging in convective updrafts, rainout from convective anvils, rainout and washout from large-scale precipitation, and species-dependent release of gases upon cloud droplets freezing [*Liu et al.*, 2001]. Dry deposition is simulated with a standard resistance-in-series model dependent on local surface type and meteorological conditions [*Wang et al.*, 1998].

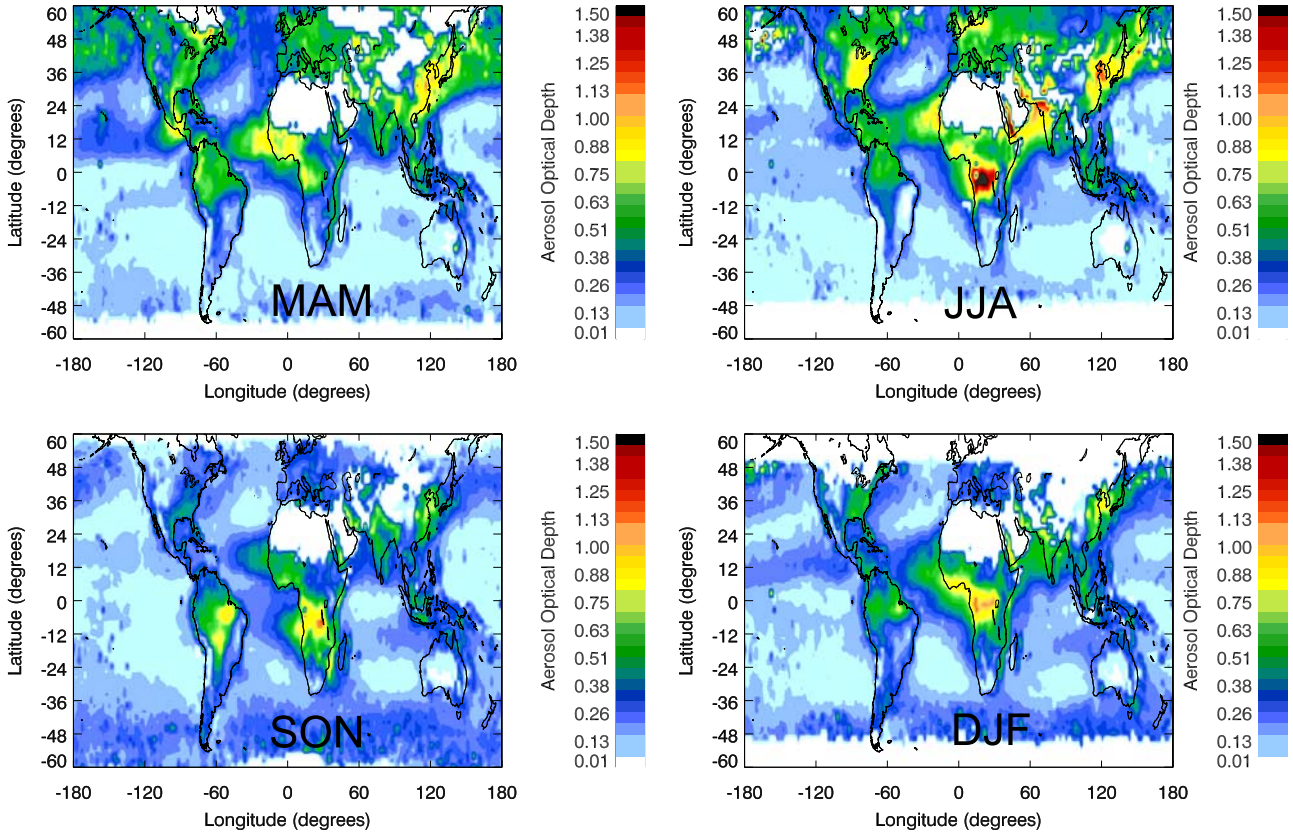

Figure 2. Seasonally averaged aerosol optical depth at 360 nm based on measurements from the MODIS satellite instrument. White areas indicate reflective regions where optical depth is not available.

[14] Of particular interest here is the simulation of the aerosol vertical profile. Figure 3 compares vertical profiles of aerosol extinction as calculated with GEOS-CHEM versus measurements from lidar. Figure 3 (top) shows a pronounced enhancement near the surface at the Atmospheric Radiation Measurements (ARM) site in both simulated and measured values throughout the year. In contrast, measured and simulated extinction profiles in the model values in South Korea are more evenly mixed throughout the troposphere. The simulation reveals that the local extinction during April is dominated by mineral dust in the free troposphere and by sulfate near the surface.

2.4. Retrieval

[15] Our retrieval calculates the column effective ω_0 necessary to reproduce the observed TOMS aerosol index, given the observed MODIS aerosol optical depth and the modeled aerosol relative vertical distribution. It uses a look-up table of backscattered radiances at two ultraviolet wavelengths (331 nm and 360 nm) for a variety of atmospheric and surface conditions as a function of all Sun-satellite viewing geometries. The radiative transfer model VLIDORT [*Natraj et al.*, 2007; Spurr, submitted manuscript, 2006] is used to create radiances for the look-up table. VLIDORT is a multiple scattering multilayer vector discrete ordinate model that will return the Stokes vector for polarized light at any optical depth and viewing geometry. The model also has a pseudospherical treatment of the solar beam in a curved spherical shell atmosphere [see, e.g., *Spurr*, 2002]. VLIDORT also has a multiple solar angle computation facility, so that one call to the model will return radiances for the complete range of solar and satellite-viewing geometries used in the look-up table. The surface is assumed to be Lambertian, based on surface albedo data set determined from TOMS by *Herman et al.* [1997]. The size distribution of aerosols is assumed to be lognormal with mode radius and standard deviation used in GEOS-CHEM [*Martin et al.*, 2003]. The optical properties of aerosols are characterized by the spectral extinction coefficient, ω_0 and the phase function which is represented by the moments of Legendre expansion polynomials. We use a Mie scattering algorithm [*Mie*, 1908] for spherical particles and the T-Matrix algorithm [*Mishchenko et al.*, 1995] for nonspherical dust particles to calculate the optical quantities.

[16] Table 1 presents the refractive indices of pure aerosol types at 360 nm and 331 nm in this study. Refractive indices of pure sulfate, soot, dust and sea salt are based on *Toon et al.* [1976], *d'Almeida et al.* [1991], and *Schuster et al.* [2005]. As the complex refractive index of dust aerosols is quite variable [*Sokolik and Toon*, 1999] in regions dominated by mineral dust, the refractive index at 360 nm is allowed to vary from 0.004 [i.e., *Colarco et al.*, 2002] to 0.02 [i.e., *Patterson et al.*, 1977] with a step size of 0.002. Following *Colarco et al.* [2002]; the value at 331 nm is set to be 20% larger than the value at 360 nm.

[17] The look-up table is searched through all possible combinations of either fraction of soot or the complex refractive index of dust to match the observed TOMS aerosol index. The dust refractive index is the free parameter in

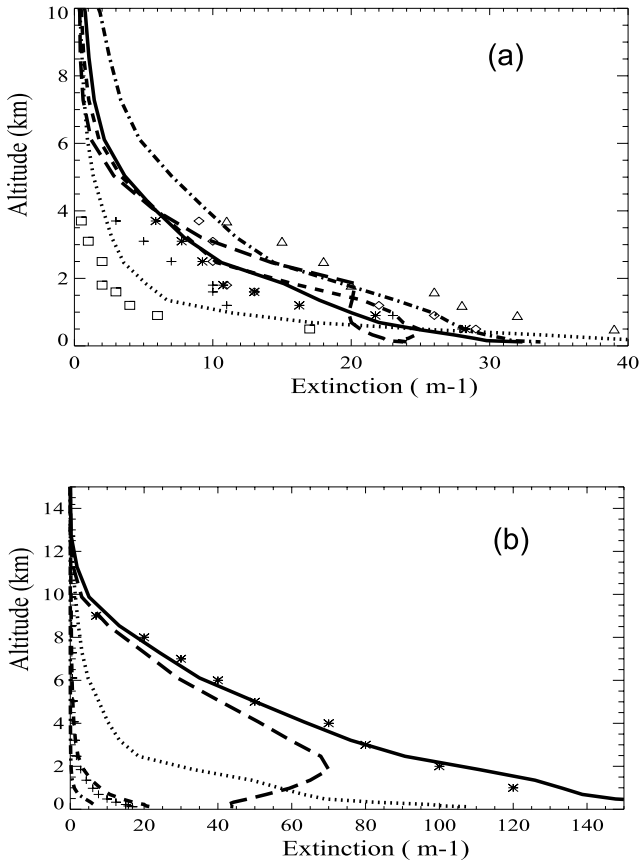

Figure 3. (a) Comparison of GEOS-CHEM simulations (lines) with lidar profiles (symbols) measured at Southern Great Plains, Lamont, Oklahoma (DOE/ARM site), for March 2000 to February 2001. Dash-dotted and diamond, MAM; long dashes and triangle, JJA; dashed and plus, SON; dotted and square, DJF; solid and asterisk, annual mean. (b) Comparison of GEOS-CHEM simulations (solid line) with in situ lidar profiles (asterisk) measured at Cheju island, South Korea in April 2000. Also shown are model calculations of extinction from each aerosol type as given by long dashes for dust, dotted for sulfate, dashed for black carbon, plus for organic carbon, and dash-dotted for sea salt.

regions dominated by mineral dust. The soot fraction is the free parameter elsewhere. Scenes with reflectivity greater than 0.2 are excluded from the retrieval to reduce cloud contamination. We use a chi-square (χ^2) minimization method to select the most likely solution following *Hu et al.* [2002]:

$$\chi^2 = \sum_j \left(\left(\mathrm{AI}_{\mathrm{measure}} - \mathrm{AI}_{\mathrm{calc},j} \right) / \sigma \right)^2 \quad (3)$$

where $\mathrm{AI}_{\mathrm{measure}}$ is the measured aerosol index, $\mathrm{AI}_{\mathrm{calc},j}$ is calculated aerosol index for possible solution j and σ is the standard deviation of the measurements. The ω_0 is determined using the dust refractive index and soot abundance that minimize χ^2.

[18] Seawater absorption of ultraviolet radiation is not well quantified due to a paucity of reliable measurements [*Vasilkov et al.*, 2002]. We identify oceanic regions where clear water absorption dominates the TOMS AI as locations where the TOMS AI exceeds 0.5 and the MODIS AOD is less than 0.25, and exclude such locations from the retrieval.

3. Results, Validation, and Discussion

[19] Figure 4 presents the retrieved ω_0 at 360 nm over midlatitude and tropical regions. We find large spatial variation in ω_0 due to aerosol composition. Values of ω_0 are near 1 over most regions of ocean where scattering sea salt and sulfate aerosols often dominate [*Chin et al.*, 2000a, 2000b]. A ω_0 of 0.89 to 0.93 at the midvisible was inferred from airborne measurements as part of the Tropospheric Aerosol Radiative Forcing Observational Experiment (TARFOX) in July 1996 over the eastern United States and western Atlantic Ocean [*Russell et al.*, 1999; *Hignett et al.*, 1999]. We find similar values during summer over and downwind of eastern North America, and more scattering aerosols during the rest of year.

[20] The retrieved ω_0 exhibits strong seasonal variation. Minimum values are associated with seasonal enhancements in mineral dust and biomass burning aerosols [*Torres et al.*, 2005], as most apparent during MAM and JJA in the Northern Hemisphere and during SON and DJF in the Southern Hemisphere. The lower value of ω_0 occurring in India during spring may be explained by seasonal biomass burning [*Duncan et al.*, 2003; *Menon et al.*, 2002; *Streets et al.*, 2003] and dust particles transported from Sahara. The seasonal minimum during spring over China is associated with frequent dust storms and long-range transport to large area of east Asia [*Zhang et al.*, 2005].

[21] Values of 0.75 to 0.9 are found in biomass burning regions of central Africa, South America, western North America and eastern Asia. Such values are broadly consistent with recent campaigns. *Dubovik et al.* [1998] retrieved ω_0 from measurements as part of the Smoke Clouds and Radiation-Brazil (SCAR-B) campaign in August and September 1995 and found a value of 0.87 at 670 nm. *Abel et al.* [2003] found a ω_0 of 0.84 to 0.9 at 550 nm in September 2000 in the aged regional haze from an agricultural fire in southern Africa during the Southern African Regional science Initiative (SAFARI 2000). *Torres et al.* [2005] found values of 0.85–0.95 in both TOMS retrievals at 380 nm and AERONET retrievals at 440 nm. The ω_0 retrieved from pyrheliometers and pyranometers in northern China between 1993 and 2001 ranged from 0.80 to 0.85 at 550 nm [*Qiu et al.*, 2004].

[22] We validate our retrieval using coincident measurements of ω_0 available from AERONET. *Dubovik et al.* [1998] retrieved ω_0 from the spectral measurements of

Table 1. Refractive Indices of Pure Aerosol Chemical Components

Wavelength, nm	Sulphate	Black Carbon	Sea Salt	Dust	Organics
360	1.45 + 0.0i	1.75 + 0.465i	1.39 + 0.0i	from 1.53 + 0.004i to 1.53 + 0.02i	1.48 + 0.005i
331	1.46 + 0.0i	1.75 + 0.47i	1.385 + 0.0i	1.53 + i(1.2*$\mathrm{Value}_{360\ \mathrm{nm}}$)	1.48 + 0.005i

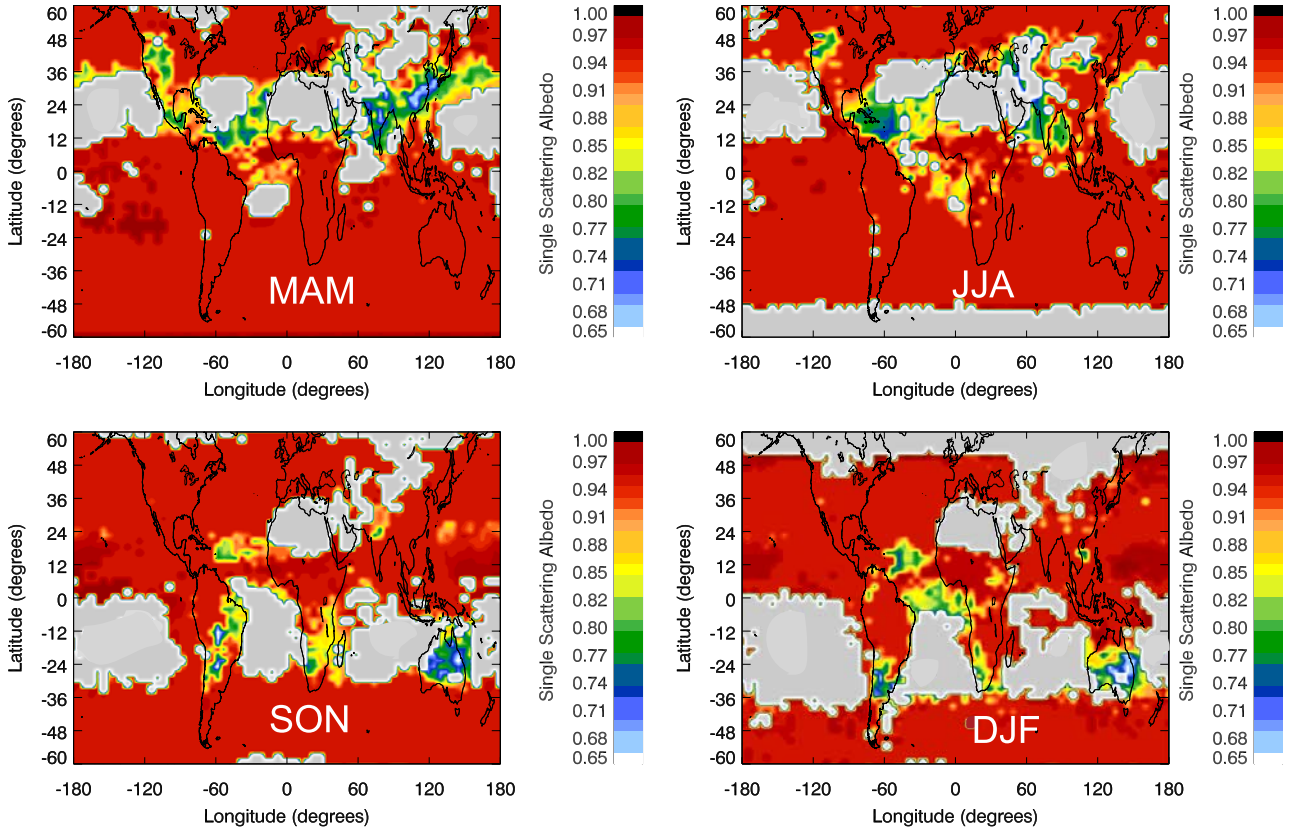

Figure 4. Seasonally averaged aerosol single scattering albedo at 360 nm retrieved from TOMS and MODIS measurements. Gray areas indicate regions where aerosol optical depth is not available from MODIS or the aerosol index is strongly influenced by absorption by clear water.

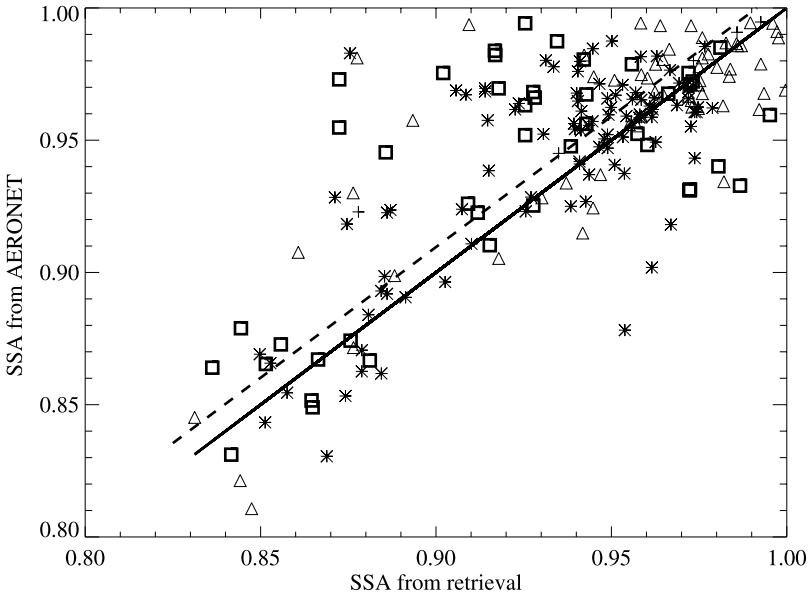

Figure 5. Comparison of coincident aerosol single scattering albedo (SSA) retrieved here with AERONET for March 2000 to February 2001 (square, MAM; asterisk, JJA; triangle, SON; plus, DJF). The solid line represents the $y = x$ line. The dashed line was calculated with organic regression [*Hirsh and Gilroy*, 1984].

Table 2. Estimate of the Uncertainty in Retrieved ω_0

Parameter	Input Uncertainty	Retrieval Uncertainty
MODIS AOD	20% ±0.05 land 5% ±0.03 ocean	±0.08
Surface reflectivity	±0.01	±0.02
Measured TOMS AI	±1%	±0.01
Angstrom exponent	±15%	±0.1
Profile	±25%	±0.05
Refractive index	±0.01	±0.02
Combined		±0.15

direct and diffuse radiations using a radiative transfer code which accounts for multiple scattering [*Nakajima et al.*, 1983]. The expected accuracy is 10–15%. We linearly extrapolate the ω_0 at AERONET wavelengths to ω_0 at TOMS wavelengths to account for the spectral dependence of the ω_0 by least squares method. All Level 2 data which are available in North America are used. Figure 5 compares our retrieved ω_0 with that determined from AERONET for the year of 2000. Both data sets exhibit a high degree of consistency with a correlation coefficient of 0.75, a slope of 0.99, and an intercept of 0.02.

4. Uncertainty Analysis

[23] Table 2 identifies the major sources of error in the retrieval and summarizes their individual contribution. We estimate the sensitivity of retrieved ω_0 to uncertainty in aerosol optical depth and surface reflectivity by conducting a synthetic retrieval of ω_0 over a range of values and subsequently examining its performance. Figure 6 shows that the uncertainty of retrieved ω_0 decreases with increasing aerosol optical depth. The MODIS retrieved aerosol optical depth contains considerable uncertainties due to assumed aerosol models, even though the aerosol models were dynamically selected by the algorithms [*Jeong et al.*, 2005]. As discussed in section 2.2, the uncertainty in the MODIS aerosol optical depth is 20% ± 0.05 over land [*Chu et al.*, 2002] and 5% ± 0.03 over ocean [*Remer et al.*, 2002]. The corresponding error in our retrieval is spatially variable with a typical value of ± 0.08. Uncertainty in surface reflectivity results in a typical uncertainty in ω_0 of less than 0.02. The radiometric errors in the TOMS instrument are less than 1% [*Levelt et al.*, 2000], yielding a typical uncertainty in ω_0 of 0.01.

[24] As discussed in section 2.2, we used the Ångström exponents from AERONET to relate the MODIS optical depth at 470 nm to ultraviolet wavelengths. However, measurements are sparse, especially in oceanic regions. Furthermore the AERONET Ångström exponent is determined from transmittance while TOMS and MODIS measure reflectance. An alternative is to substitute the values over the ocean with the Ångström exponents from MODIS measurements at 470 nm and 660 nm. These two methods can lead to the difference of our retrieval results of 11%.

[25] Because of atmospheric scattering, the aerosol profile also influences the backscattered radiance calculation and the retrieved ω_0. Previous evaluation of the GEOS-CHEM aerosol simulation by *Park et al.* [2005] found little bias in the vertical profile for black carbon and sulfate-nitrate-ammonium aerosols. *Heald et al.* [2005] found consistency between measured and simulated organic aerosol in the lower troposphere, but the model underestimates free tropospheric organic aerosol by a factor of 10–100. Figure 3 shows that simulated and measured aerosol extinctions often agree to better than 25%. We conduct a sensitivity analysis to assess the model contribution to the retrieval by using a global mean aerosol profile instead of the locally varying profiles. Most regions show differences of less than 0.05.

[26] The retrieved ω_0 is sensitive to the refractive index. Organic aerosols could be more absorbing in the ultraviolet than assumed here if the aerosols contain chromophore functional groups [*Jacobson*, 1999]. A sensitivity test in which the imaginary part of the refractive index is doubled changes the retrieved ω_0 by ± 0.02.

[27] Considering possible sources of uncertainty, our retrievals can reach the accuracy to ± 15%. The Ångström exponent makes the largest contribution to the retrieval uncertainty at higher value of aerosol optical depth, and the optical depth makes the largest uncertainty of retrieval at lower value of aerosol optical depth.

5. Conclusions

[28] We present a new approach to retrieve the column effective aerosol single scattering albedo (ω_0) from space-based observations of backscattered radiance. The TOMS aerosol index provides the ω_0 sensitive measurement. Coincident observations of aerosol optical depth from the MODIS satellite instrument and simulations of the aerosol vertical profile with a chemical transport model (GEOS-CHEM) constrain other parameters to which the TOMS aerosol index is sensitive. The column effective ω_0 is determined as the value that minimizes the difference between the calculated and observed aerosol index.

[29] We evaluate the GEOS-CHEM aerosol simulation with vertical profiles of aerosol extinction measured from lidar at DOE/ARM site in Oklahoma and at Cheju Island in South Korea. The simulated and observed profiles are

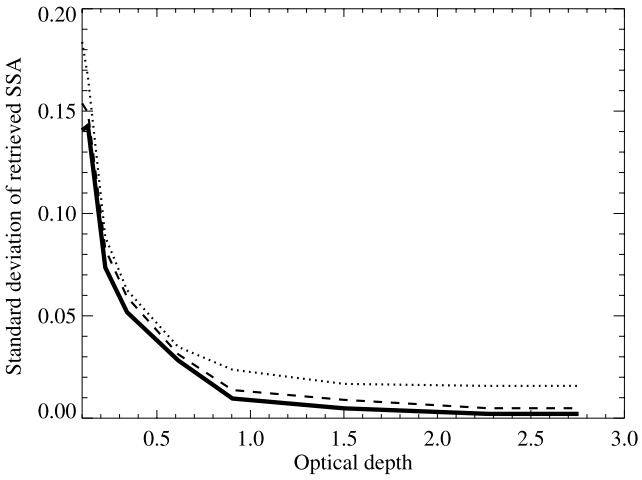

Figure 6. Standard deviation of single scattering albedo (SSA) between retrieved and synthetic values for testing our retrieval method how sensitive to the aerosol optical depth. Solid, surface reflectivity 0.05; dashed, surface reflectivity 0.08; dotted, surface reflectivity 0.15.

highly consistent. Maximum differences are found at the ARM site during winter when the observed values are a factor of 2 lower than the simulated values.

[30] Our retrieved ω_0 at 360 nm shows values near 1 over the remote oceans, where the aerosol burden is dominated by sea salt. Lower values of ω_0 near 0.8 are found over regions of biomass burning and mineral dust such as northern Africa, the northern tropical Atlantic, and the Middle East. Seasonal minima are found over East Asia and South Asia during spring associated with both mineral dust and biomass burning.

[31] We validate our retrieval using coincident observations from the Aerosol Robotic Network (AERONET) over North America. The two data sets exhibit a high degree of consistency with a correlation coefficient of 0.75, slope of 0.99 and intercept of 0.02. We conduct a variety of sensitivity analyses to assess the retrieval uncertainty. The dominant terms are the Ångström exponent, the aerosol optical depth and aerosol profiles contributing to a total uncertainty of 15%. The retrieval uncertainty decreases with increasing aerosol optical depth, suggesting that our retrieval procedure works better in more turbid atmosphere. Additional constraints on aerosol vertical profile from the CALIPSO satellite [*Winker et al.*, 2003] would improve future retrievals of ω_0. Further characterization of seawater absorption at ultraviolet wavelengths should improve retrievals over ocean.

[32] Additional concerns in the current work are errors introduced by using two satellite instruments with different spatial resolution, slightly different observation times, and different calibrations. Future design of a single satellite instrument that has very high spatial resolution for cloud clearing, and includes ultraviolet wavelengths, would enable retrieval of ω_0 for individual scenes.

[33] **Acknowledgments.** We would like to thank the scientists and managers for making the TOMS, MODIS, and AERONET data publicly available. We are grateful to Aaron Van Donkelaar for computational algorithms. Norm O'Neill, Oleg Dubovik, Omar Torres, and two anonymous reviewers provided valuable comments that improved the manuscript. We would like to thank Robert Spurr of RT Solutions, Inc. for the use of his VLIDORT radiative transfer model. This work was supported by the Canadian Foundation for Climate and Atmospheric Science as part of the Multiscale Air Quality Modeling Network. The GEOS-CHEM model is managed by the Atmospheric Chemistry Modeling group at Harvard University with support from the NASA Atmospheric Chemistry Modeling and Analysis Program.

References

Abel, S. J., J. M. Haywood, E. J. Highwood, J. Li, and P. R. Buseck (2003), Evolution of biomass burning aerosol properties from an agricultural fire in southern Africa, *Geophys. Res. Lett.*, *30*(15), 1783, doi:10.1029/2003GL017342.

Ackerman, A. S., O. B. Toon, D. E. Stevens, A. J. Heymsfield, V. Ramanathan, and E. J. Welton (2000), Reduction of tropical cloudiness by soot, *Science*, *288*, 1042–1047.

Alexander, B., R. J. Park, D. J. Jacob, Q. B. Li, R. M. Yantosca, J. Savarino, C. C. W. Lee, and M. H. Thiemens (2005), Sulfate formation in sea-salt aerosols: Constraints from oxygen isotopes, *J. Geophys. Res.*, *110*, D10307, doi:10.1029/2004JD005659.

Bey, I., D. J. Jacob, J. A. Logan, and R. M. Yantosca (2001), Asian chemical outflow to the Pacific: Origins, pathways, and budgets, *J. Geophys. Res.*, *106*, 23,097–23,114.

Chin, M., R. B. Rood, S.-J. Lin, J.-F. Muller, and A. M. Thompson (2000a), Atmospheric sulfur cycle simulated in the global model GOCART: Model description and global properties, *J. Geophys. Res.*, *105*, 24,671–24,687.

Chin, M., D. L. Savoie, B. J. Huebert, A. R. Bandy, D. C. Thornton, T. S. Bates, P. K. Quinn, E. S. Saltzman, and W. J. De Bruyn (2000b), Atmospheric sulfur cycle simulated in the global model GOCART: Comparison with field observations and regional budgets, *J. Geophys. Res.*, *105*, 24,689–24,712.

Chu, D. A., Y. J. Kaufman, C. Ichoku, L. A. Remer, D. Tanré, and B. N. Holben (2002), Validation of MODIS aerosol optical depth retrieval over land, *Geophys. Res. Lett.*, *29*(12), 8007, doi:10.1029/2001GL013205.

Chu, D. A., Y. J. Kaufman, G. Zibordi, J. D. Chern, J. Mao, C. Li, and B. N. Holben (2003), Global monitoring of air pollution over land from the Earth Observing System-Terra Moderate Resolution Imaging Spectroradiometer (MODIS), *J. Geophys. Res.*, *108*(D21), 4661, doi:10.1029/2002JD003179.

Chu, D.A., et al. (2005), Evaluation of aerosol properties over ocean from Moderate Resolution Imaging Spectroradiometer (MODIS) during ACE-Asia, *J. Geophys. Res.*, *110*, D07308, doi:10.1029/2004JD005208.

Chylek, P., G. Videen, D. Ngo, R. Pinnick, and J. Klett (1995), Effect of black carbon on the optical properties and climate forcing of sulfate aerosols, *J. Geophys. Res.*, *100*, 16,325–16,332.

Colarco, P. R., O. B. Toon, O. Torres, and P. J. Rasch (2002), Determining the UV imaginary index of refraction of Saharan dust particles from Total Ozone Mapping Spectrometer data using a three-dimensional model of dust transport, *J. Geophys. Res.*, *107*(D16), 4289, doi:10.1029/2001JD000903.

d'Almeida, G. A., P. Koepke, and E. P. Shettle (1991), *Atmospheric Aerosols: Global Climatology and Radiative Characteristics*, 561 pp., A. Deepak, Hampton, Va.

de Graaf, M., P. Stammes, O. Torres, and R. B. A. Koelemeijer (2005), Absorbing Aerosol Index: Sensitivity analysis, application to GOME and comparison with TOMS, *J. Geophys. Res.*, *110*, D01201, doi:10.1029/2004JD005178.

Dubovik, O., B. N. Holben, Y. J. Kaufman, M. Yamasoe, A. Smirnov, D. Tanré, and I. Slutsker (1998), Single-scattering albedo of smoke retrieved from the sky radiance and solar transmittance measured from ground, *J. Geophys. Res.*, *103*, 31,903–31,923.

Dubovik, O., B. N. Holben, T. F. Eck, A. Smirnov, Y. J. Kaufman, D. Tanré, and I. Slutsker (2002), Variability of absorption and optical properties of key aerosol types observed in worldwide locations, *J. Atmos. Sci.*, *59*, 590–608.

Duncan, B. N., R. V. Martin, A. C. Staudt, R. Yevich, and J. A. Logan (2003), Interannual and seasonal variability of biomass burning emissions constrained by satellite observations, *J. Geophys. Res.*, *108*(D2), 4100, doi:10.1029/2002JD002378.

Fairlie, T. D., D. J. Jacob, and R. J. Park (2006), The impact of trans-Pacific transport of mineral dust in the United States, *Atmos. Environ*, in press.

Ginoux, P., and O. Torres (2003), Empirical TOMS index for dust aerosol: Applications to model validation and source characterization, *J. Geophys. Res.*, *108*(D17), 4534, doi:10.1029/2003JD003470.

Ginoux, P., M. Chin, I. Tegen, J. Prospero, B. Holben, O. Dubovik, and S.-J. Lin (2001), Sources and distributions of dust aerosols simulated with the GOCART model, *J. Geophys. Res.*, *106*, 20,555–20,273.

Gong, S. L., L. A. Barrie, and J.-P. Blanchet (1997), Modeling sea-salt aerosols in the atmosphere: 1. Model development, *J. Geophys. Res.*, *102*, 3805–3818.

Hansen, J. E., M. Sato, and R. Ruedy (1997), Radiative forcing and climate response, *J. Geophys. Res.*, *102*, 6831–6864.

Haywood, J. M., and K. P. Shine (1995), The effect of anthropogenic sulfate and soot on the clear sky planetary radiation budget, *Geophys. Res. Lett.*, *22*, 603–606.

Heald, C. L., D. J. Jacob, R. J. Park, L. M. Russell, B. J. Huebert, J. H. Seinfeld, H. Liao, and R. J. Weber (2005), A large organic aerosol source in the free troposphere missing from current models, *Geophys. Res. Lett.*, *32*, L18809, doi:10.1029/2005GL023831.

Herman, J. R., P. K. Bhartia, O. Torres, C. Hsu, C. Seftor, and E. Celarier (1997), Global distribution of ultraviolet-absorbing aerosols from Nimbus 7-TOMS data, *J. Geophys. Res.*, *102*, 16,911–16,922.

Hignett, P., J. P. Taylor, P. N. Francis, and M. D. Glew (1999), Comparison of observed and modelled direct aerosol forcing during TARFOX, *J. Geophys. Res.*, *104*, 2279–2288.

Hirsh, R. M., and E. J. Gilroy (1984), Methods of fitting a straight line to data: Examples in water resources, *Water Res. Bull.*, *20*, 705–711.

Holben, B. N., et al. (1998), AERONET—A federated instrument network and data archive for aerosol characterization, *Remote Sens. Environ.*, *66*, 1–16.

Hsu, N. C., J. R. Herman, P. K. Bhartia, C. J. Seftor, O. Torres, A. M. Thompson, J. F. Gleason, T. F. Eck, and B. N. Holben (1996), Detection of biomass burning smoke from TOMS measurements, *Geophys. Res. Lett.*, *23*, 745–748.

Hsu, N. C., J. R. Herman, O. Torres, B. N. Holben, D. Tanr, T. F. Eck, A. Smirnov, B. Chatenet, and F. Lavenu (1999), Comparisons of the TOMS aerosol index with Sun-photometer aerosol optical thickness: Results and applications, *J. Geophys. Res.*, *104*, 6269–6279.

Hu, R.-M., K. S. Carslaw, C. Hostetler, L. R. Poole, B. Luo, T. Peter, S. Füeglistaler, T. J. McGee, and J. F. Burris (2002), Microphysical properties of wave polar stratospheric clouds retrieved from lidar measurements during SOLVE/THESEO 2000, *J. Geophys. Res.*, *107*(D20), 8294, doi:10.1029/2001JD001125.

Intergovernmental Panel on Climate Change (2001), *Climate Change 2001: The Scientific Basis, Contribution of Working Group I to the Third Assessment Report of the Intergovernmental Panel on Climate Change*, edited by J. T. Houghton et al., Cambridge Univ. Press, New York.

Jacob, D. J. (2000), Heterogeneous chemistry and troposheric ozone, *Atmos. Environ.*, *34*, 2131–2159.

Jacobson, M. Z. (1999), Isolating nitrated and aromatic aerosols and nitrated aromatic gases as sources of ultraviolet light absorption, *J. Geophys. Res.*, *104*, 3527–3542.

Jeong, M.-J., Z. Li, D. A. Chu, and S.-C. Tsay (2005), Quality and compatibility analyses of global aerosol products derived from the advanced very high resolution radiometer and Moderate Resolution Imaging Spectroradiometer, *J. Geophys. Res.*, *110*, D10S09, doi:10.1029/2004JD004648.

Kaufman, Y. J., D. Tanré, L. A. Remer, E. F. Vermote, A. Chu, and B. N. Holben (1997), Operational remote sensing of tropospheric aerosol over land from EOS moderate resolution imaging spectroradiometer, *J. Geophys. Res.*, *102*, 17,051–17,067.

Kaufman, Y. J., J. V. Martins, L. A. Remer, M. R. Schoeberl, and M. A. Yamasoe (2002a), Satellite retrieval of aerosol absorption over the oceans using sunglint, *Geophys. Res. Lett.*, *29*(19), 1928, doi:10.1029/2002GL015403.

Kaufman, Y. J., D. Tanré, and O. Boucher (2002b), A satellite view of aerosols in the climate system, *Nature*, *419*, 215–223.

Kaufman, Y. J., I. Koren, L. A. Remer, D. Tanré, P. Ginoux, and S. Fan (2005), Dust transport and deposition observed from the Terra-Moderate Resolution Imaging Spectroradiometer (MODIS) spacecraft over the Atlantic Ocean, *J. Geophys. Res.*, *110*, D10S12, doi:10.1029/2003JD004436.

King, M. D., Y. J. Kaufman, D. Tanre, and T. Nakajima (1999), Remote sensing of tropospheric aerosols from space: Past, present, and future, *Bull. Am. Meteorol. Soc.*, *80*, 2229–2259.

Levelt, P. F., et al. (2000), *Science Requirements Document for OMI-EOS, RS-OMIE-KNMI-001*, version 2, *KNMI Publ. 193*, R. Neth. Meteorol. Inst., De Bilt, Netherlands.

Li, Z., and L. Kou (1998), The direct radiative effect of smoke aerosols on atmospheric absorption of visible sunlight, *Tellus, Ser. B.*, *50*, 543–554.

Litjens, R. A. J., T. I. Quickenden, and C. G. Freeman (1999), Visible and near-ultraviolet absorption spectrum of liquid water, *Appl. Opt.*, *38*(7), 1216–1223.

Liu, H., D. J. Jacob, I. Bey, and R. M. Yantosca (2001), Constraints from 210Pb and 7Be on wet deposition and transporting a global three-dimensional chemical tracer model driven by assimilated meteorological fields, *J. Geophys. Res.*, *106*, 12,109–12,128.

Martin, R. V., D. J. Jacob, R. M. Yantosca, M. Chin, and P. Ginoux (2003), Global and regional decreases in tropospheric oxidants from photochemical effects of aerosols, *J. Geophys. Res.*, *108*(D3), 4097, doi:10.1029/2002JD002622.

Martins, J. V., D. Tanr, L. Remer, Y. Kaufman, S. Mattoo, and R. Levy (2002), MODIS Cloud screening for remote sensing of aerosols over oceans using spatial variability, *Geophys. Res. Lett.*, *29*(12), 8009, doi:10.1029/2001GL013252.

Menon, S., J. Hansen, L. Nazarenko, and Y. Luo (2002), Climate effects of black carbon aerosols in China and India, *Science*, *297*, 2250–2253.

Mie, G. (1908), Beitrage zur Optik truber Medien, speziell Kolloidaler Metallosungen, *Ann. Phys.*, *25*, 377–445.

Mishchenko, M. I., A. A. Lacis, B. E. Charlson, and L. D. Tavis (1995), Nonsphericity of dust-like tropospheric aerosols: Implications for aerosol remote sensing and climate modeling, *Geophys. Res. Lett.*, *22*, 1077–1080.

Nakajima, T., M. Tanaka, and T. Yamauchi (1983), Retrieval of the optical properties of aerosols from aureole and extinction data, *Appl. Opt.*, *22*, 2951–2959.

Natraj, V., R. Spurr, H. Boesch, Y. Jiang, and Y. Yung (2007), Evaluation of errors in neglecting polarization in the forward modeling of O_2 A band measurements from space, with relevance to CO_2 column retrieval from polarization sensitive instruments, *J. Quant. Spectrosc. Radiat. Transfer*, *103*(2), 245–259.

O'Reilly, J. E., S. Maritorena, B. G. Mitchell, D. A. Siegel, K. L. Carder, S. A. Garver, M. Kahru, and C. McClain (1998), Ocean color chlorophyll algorithms for SeaWiFS, *J. Geophys. Res.*, *103*, 24,937–24,954.

Park, R. J., D. J. Jacob, B. D. Field, R. M. Yantosca, and M. Chin (2004), Natural and transboundary pollution influences on sulfate-nitrate-ammonium aerosols in the United States: Implications for policy, *J. Geophys. Res.*, *109*, D15204, doi:10.1029/2003JD004473.

Park, R. J., et al. (2005), Export efficiency of black carbon aerosol in continental outflow: Global implications, *J. Geophys. Res.*, *110*, D11205, doi:10.1029/2004JD005432.

Patterson, E. M., D. A. Gillette, and B. H. Stockton (1977), Complex index of refraction between 300 and 700 nm for Sahara aerosols, *J. Geophys. Res.*, *82*, 3153–3160.

Penner, J. E., C. C. Chuang, and K. Grant (1998), Climate forcing by carbonaceous and sulfate aerosols, *Clim. Dyn.*, *14*, 839–851.

Qiu, J., L. Yang, and X. Zhang (2004), Characteristics of the imaginary part and single-scattering albedo of urban aerosols in northern China, *Tellus, Ser. B.*, *56*, 276–284.

Ramanathan, V., P. J. Crutzen, J. T. Kiehl, and D. Rosenfeld (2001), Aerosol, climate, and hydrological cycle, *Science*, *294*, 2119–2124.

Remer, L. A., et al. (2002), Validation of MODIS aerosol retrieval over ocean, *Geophys. Res. Lett.*, *29*(12), 8008, doi:10.1029/2001GL013204.

Russell, P. B., P. V. Hobbs, and L. L. Stowe (1999), Aerosol properties and radiative effects in the United States east coast haze plume: An overview of the Tropospheric Aerosol Forcing Observational Experiment (TARFOX), *J. Geophys. Res.*, *104*, 2213–2222.

Schuster, G. L., O. Dubovik, B. N. Holben, and E. E. Clothiaux (2005), Inferring black carbon content and specific absorption from Aerosol Robotic Network (AERONET) aerosol retrievals, *J. Geophys. Res.*, *110*, D10S17, doi:10.1029/2004JD004548.

Sokolik, I. N., and O. B. Toon (1999), Incorporation of mineralogical composition into models of the radiative properties of mineral aerosol from UV to IR wavelengths, *J. Geophys. Res.*, *104*, 9423–9444.

Spurr, R. J. D. (2002), Simultaneous derivation of intensities and weighting functions in a general pseudo-spherical discrete ordinate radiative transfer treatment, *J. Quant. Spectrosc. Radiat. Transfer*, *75*, 129–175.

Streets, D. G., et al. (2003), An inventory of gaseous and primary aerosol emissions in Asia in the year 2000, *J. Geophys. Res.*, *108*(D21), 8809, doi:10.1029/2002JD003093.

Tanré, D., Y. J. Kaufman, M. Herman, and S. Matoo (1997), Remote sensing of aerosol properties over oceans using the MODIS/EOS spectral radiances, *J. Geophys. Res.*, *102*, 16,971–16,988.

Toon, O., J. Pollack, and B. Khare (1976), The optical constants of several atmospheric species: Ammonium sulfate, ammonium oxide and sodium chloride, *J. Geophys. Res.*, *81*, 5733–5748.

Torres, O., P. K. Bhartia, J. R. Herman, Z. Ahmad, and J. Gleason (1998), Derivation of aerosol properties from satellite measurements of backscattered ultraviolet radiation: Theoretical basis, *J. Geophys. Res.*, *103*, 17,099–17,110.

Torres, O., P. K. Bhartia, J. R. Herman, A. Sinyuk, P. Ginoux, and B. Holben (2002), A long-term record of aerosol optical depth from TOMS observations and comparison to AERONET measurements, *J. Atmos. Sci.*, *59*, 398–413.

Torres, O., P. K. Bhartia, A. Sinyuk, E. J. Welton, and B. Holben (2005), Total Ozone Mapping Spectrometer measurements of aerosol absorption from space: Comparison to SAFARI 2000 ground-based observations, *J. Geophys. Res.*, *110*, D10S18, doi:10.1029/2004JD004611.

Vasilkov, A. P., et al. (2002), Problems in assessment of the ultraviolet penetration into natural waters from space-based measurements, *Opt. Eng.*, *41*(12), 3019–3027.

Wang, Y., D. J. Jacob, and J. A. Logan (1998), Global simulation of tropospheric O3-NOx-hydrocarbon chemistry: 1. Model formulation, *J. Geophys. Res.*, *103*, 10,713–10,726.

Winker, D. M., J. Pelon, and M. P. McCormick (2003), The CALIPSO mission: Spaceborne lidar for observation of aerosols and clouds, *Proc. SPIE*, *4893*, 1–11.

Zender, C. S., H. Bian, and D. Newman (2003a), Mineral Dust Entrainment and Deposition (DEAD) model: Description and 1990s dust climatology, *J. Geophys. Res.*, *108*(D14), 4416, doi:10.1029/2002JD002775.

Zender, C. S., D. Newman, and O. Torres (2003b), Spatial heterogeneity in aeolian erodibility: Uniform, topographic, geomorphic, and hydrologic hypotheses, *J. Geophys. Res.*, *108*(D17), 4543, doi:10.1029/2002JD003039.

Zhang, D., Y. Iwasaka, G. Shi, J. Zang, M. Hu, and C. Li (2005), Separated status of the natural dust plume and polluted air masses in an Asian dust storm event at coastal areas of China, *J. Geophys. Res.*, *110*, D06302, doi:10.1029/2004JD005305.

T. D. Fairlie, NASA Langley Research Center, MS 401B, Hampton, VA 23681, USA.

R.-M. Hu and R. V. Martin, Department of Physics and Atmospheric Science, Dalhousie University, Halifax, NS, Canada B3H 3J5. (hu@fizz.phys.dal.ca)